



Modeling of a novel K5 prism-based surface Plasmon resonance sensor for urea detection employing Aluminum arsenide

Yesudasu Vasimalla¹ · Himansu Shekhar Pradhan¹

Received: 27 January 2022 / Accepted: 11 April 2022 / Published online: 14 May 2022
© The Author(s), under exclusive licence to The Optical Society of India 2022

Abstract This paper presents the modeling of a novel Kron-5 (K5) prism-based Surface Plasmon Resonance (SPR) sensor to detect urea employing Aluminum arsenide (AIAs). The proposed SPR structure is designed based on a silver (Ag)-coated Kretschmann configuration. This structure contains AIAs to avoid Ag oxidation, as well as barium titanate for increased absorption, and black phosphorus for biorecognition element, respectively. For the detection process, the urea concentration of 0.625 gm/dl, 2.5 gm/dl and 5 gm/dl are used with the refractive indices (RIs) of 1.337, 1.339 and 1.342, respectively. The presented work is shown in three significant ways at 633 nm wavelength by exploiting the transfer matrix method. Firstly, the optimal performance of the proposed K5 prism-based structure is compared with BK7 and SK11-based structures, which have lower and higher refractive indexes compared to the proposed prism. Secondly, the optimal performance of the proposed structure is validated with respect to the RI of urea. Thirdly, an impact of AIAs in the proposed structure has been shown. The maximum achieved SPR parameters are sensitivity of $452.85^\circ/\text{RIU}$, quality factor of 93.37 RIU^{-1} , detection accuracy of 0.65 and dip-of-figure-of-merit of 129,388.57 for the proposed sensor. Finally, the comparative study of SPR sensor performance for urea detection is presented.

Keywords Aluminum arsenide · Barium titanate · Kretschmann configuration · Sensitivity · SPR biosensor · Urea detection

Introduction

The kidneys play a crucial function in human health. They are both biologically beneficial and highly complex systems of waste disposal. They can examine a continuous sorting process of non-recyclable waste from recyclable waste, and also, they can clean the blood by filtering the poisons and pollutants. To form urine, the kidneys take out waste and excess water from the bloodstream. Urine passes out from the kidneys to the bladder through the ureter. The rest of the blood originate from the food and active muscle. After the body receives what is necessary from the food for generating energy and for repair themselves, waste is forward to the blood. In this event, if the kidneys do not remove the wastes, then they will build up in the blood and harm the human body. Urea is a waste material that produced from the protein breakdown in the blood and released in the urine. The presence of high urea levels in the blood implies that the kidneys are not working properly. In such case, an artificial kidney or hemodialysis can be used to get proper function of kidney. Therefore, appropriate sensing systems are required to detect the adequate waste disposal, including urea [1].

The surface plasmon resonance (SPR) sensor is a most promising optical device for monitoring biomolecules in clinical samples, including proteins, enzymes, antibodies, small molecules, drugs and peptides due to a label-free and advanced technology [2]. Moreover, it can be used as a real-time monitoring device because of its quick detection process, high sensitivity (S), accuracy, reliability and rapid detection techniques [3, 4]. The prism-coupled, optical

✉ Yesudasu Vasimalla
dasu_719075@student.nitw.ac.in

Himansu Shekhar Pradhan
hsp@nitw.ac.in

¹ National Institute of Technology, Warangal,
Telangana 506004, India

fibre-coupled and waveguide-coupled are the various types of SPR sensors can be designed based on their light coupling mechanism. In comparison to waveguide and fibre optic coupling, the prism coupling sensor demands greater light alignment. Moreover, remote sensing applications in hazardous locations are not attracted to prism-based SPR sensors. [5]. But, it provides the accurate realization, whereas other sensors suffer from the proper light coupling. However, all the sensors have their own merits and demerits [6]. Furthermore, the SPR sensor is considered into two configurations to simulate the leaky or guided waves: (i) Kretschmann that contains a metal film-coated prism surface (ii) Otto, having some air gap between the prism-metal (P-M) interfaces. Many researchers prefer the Kretschmann configuration because it has high efficient light coupling from prism to metal film [7]. The SPR structure, in general, uses gold (Au) and silver (Ag) as metal sheets to excite surface plasmons (SPs) on the prism's surface. Each metal has its own set of benefits and drawbacks. This work considers the Ag as the metal film for the proposed structure because of its high SPR ratio (the ratio of a dielectric constant's real and imaginary absolute values), indicating better S [8]. Moreover, it offers a sharp SPR curve that signifies less full width half maximum (FWHM), enhancing the SPR performance in terms of quality factor [9, 10]. In the SPR sensing process, an incident electromagnetic wave (EMW) passes via prism at an angle greater than the critical angle. The EMW moves more quickly through the lower refractive indices glasses, such as Kron (K5), borosilicate glass (BK7) and Schwer Kron11 (SK11) prisms. The ratio of resonance angle changes and RI changes is called the S, a key parameter for better performance in SPR-based sensor [11]. In order to analyze the SPR sensor, many researchers have suggested the angular interrogation strategy for the S measurements [12].

Furthermore, single metal film-coated SPR sensors furnish low S, but the higher S is the author's ultimate goal [13]. It has been found in the literature that many researchers have proposed hybrid structures for the SPR sensor using different combinations of dielectric materials in order to enhance S [13–17]. In addition, other researchers have already presented the SPR sensors for urea detection using dielectric material-based structures [18, 19]. However, succession is still a prerequisite for the researchers. Therefore, to improve the SPR performance, this work introduces a new dielectric material of aluminum arsenide (AlAs) for urea detection. It can enhance the S of SPR sensor due to its super-lattice structure, resulting in its semiconductor properties, such as high thermal conductivity, superior performance, and broader bandgap. Moreover, the SPR structures need to sustain the large-scale binding as well as adsorbents in order to obtain a larger resonance shift to

enhance the performance [20]. Hence, the barium titanate (BaTiO_3) is a family of promising 2D materials that can enhance resonance shift due to unusual spawning properties like low dielectric losses and high RI. It comprises of an acceptable material for enhancing the performance of SPR by considering minute variation of sensing RI that lead to higher S [21–23]. Moreover, black phosphorus (BP) is also a promising two-dimensional (2D) material and widely recognized Nano-material in photonic sensors due to its high adsorption capacity (that efficiently matches the binding biomolecules), distinctive mechanical and opto-electrical properties [24–27]. Several high performing SPR biosensors are proposed using these exceptional properties of BP and BaTiO_3 -based structures in the literature [28–30]. N. Mugdal et al. have been presented the SF-10 prism-based SPR sensor and found maximum sensitivity is obtained as $116.67^\circ/\text{RIU}$ for zinc oxide-Ag-Au- BaTiO_3 structure [31]. Moreover, high-sensitivity performance of BK7 prism-based SPR sensor has been proposed by A. Pal et al. employing graphene and BaTiO_3 structure. Four thin layers of BaTiO_3 and a single layer of graphene were used to obtain a sensitivity of $280^\circ/\text{RIU}$, which is 108 percent greater than the typical sensor [32]. BK7-Ag- BaTiO_3 -graphene-based SPR sensor has been presented with the sensitivity of $257^\circ/\text{RIU}$, where Ag thickness is 45 nm [21]. Recently, K. Bishma et al. have been proposed a remarkable BK7 prism-based SPR sensor performance employing Ag and BaTiO_3 and BP structure. They have obtained that the maximum sensitivity for Ag/ BaTiO_3 /BP structure is $360^\circ/\text{RIU}$, which is 1.5 times greater than conventional SPR sensor [33]. A. Srivastava et al. have been proposed high-performance SPR sensor employing Ag- WS_2 - BaTiO_3 -BP-based structure and found highest sensitivity as $370^\circ/\text{RIU}$ [34].

Therefore, being inspired the properties of Ag, AlAs, BaTiO_3 and BP, this paper presents a unique SPR sensor to improve S performance for urea detection. The proposed structure consists of six layers: the K5-prism, Ag, AlAs, BaTiO_3 , BP and sensing medium. The paper is organized as follows: Sect. 2 explains the design consideration and methodology of the proposed sensor structure. Section 3 demonstrates the results and discussion of the proposed design. Finally, Sect. 4 concludes the presented work. The symbol and corresponding definitions are used in this paper as tabulated in Table 1.

Design consideration and methodology

In order to design the structure and analyze the performance of the proposed sensor, this section explains its design parameters and methodology.

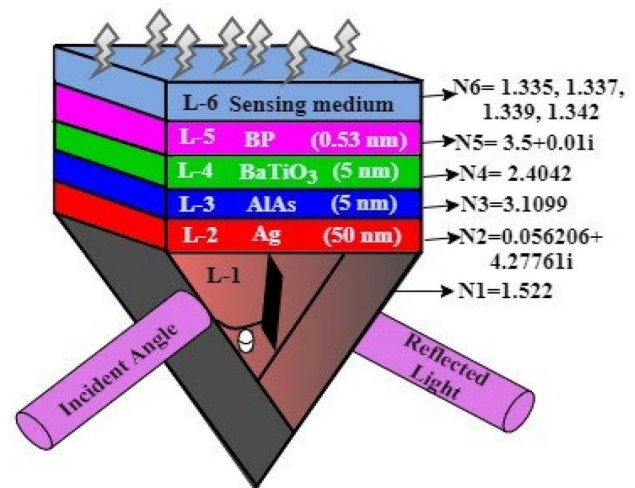
Table 1 List of symbols, notations and abbreviation

Symbol	Definition or full form
Ag	Silver
BaTiO ₃	Barium Titanate
t_k	A transverse RI
BP	Black Phosphorus
BK7	Borosilicate glass
∇n	RI Variation
FOM	Figure of merit
$\nabla\theta_{res}$	SPR resonance angle variation
FWHM	Full width half maxima
H	Characteristics matrix
nm	Nano-meter
QF	Quality factor
PC	Propagation constant
RI	Refractive index
P-M	Prism and metal
R_{min}	Minimum reflected intensity
M-D	Metal and Dielectric
R_p	Total reflected intensity
S	Sensitivity
SP	Surface Plasmons
SPW	Surface Plasmon Wave
TMM	Transfer Matrix Method
θ_k	Input angle
ϵ_k	kth layer permittivity
d_k	kth layer thickness
μ_k	kth layer permeability
z_k	kth layer impedance wave
k_x	Incident wave vector
k_{spw}	Vector of SPW
β_k	Arbitrary stage constant
λ	Wavelength

Proposed SPR design consideration

The schematic structure of the proposed SPR sensor for urea detection is depicted in Fig. 1. To compare the proposed K5 prism-based structure's performance, we have considered two other prism-based structures, namely BK7 and SK11, which are having lower and higher refractive indices compared to the proposed prism's RI. The RI of the BK7, K5 and SK11 prisms are considered as 1.5151, 1.522 and 1.564, respectively, at a wavelength (λ) of 633 nm [35].

In the designed structure, the prism is placed as a first layer to couple the incident light with λ of 633 nm. The second layer is made up of Ag, which is deployed on the prism's surface with a RI of $0.056260 + 4.2776i$, as determined by Eq. (1) [36, 37]. Where λ_c and λ_p represent the collision and plasma wavelengths, and their values are 1.7614×10^{-5} m and

**Fig. 1** The proposed SPR biosensor structure for urea detection

1.4541×10^{-7} m, respectively. The third layer is comprised of AlAs, as deposited on the Ag, having the RI of 3.1099 [38, 39]. The metal film's thickness is 50 nm that can offer less R_{min} and better SPR performance [28]. The AlAs thickness is optimized by the iteration process of Fresnel's reflectivity (R_p) mode analysis [28, 30] because the thickness nature of dielectric material is changed according to its RI [40]. Furthermore, the fourth layer is a compound of BaTiO₃, as deposited on the AlAs, having the RI of 2.4042 [31] with a thickness of 5 nm [37]. The BP is coated as the fifth layer over the BaTiO₃ with an RI of $3.5 + 0.01i$ and thickness of 0.53 nm [28]. Finally, the sixth layer is a sensing medium, having the urea's presence that can be determined by its refractive indexes, which are 1.337, 1.339 and 1.342 for the concentrations of 0.625 gm/dl, 2.5 gm/dl and 5 gm/dl, respectively [3, 38]. The RI for normal urea is determined as 1.335, and it fluctuates according to the concentration and motility of the culture [41, 42].

$$n_{AG} = \left(1 - \frac{\lambda^2 \lambda_c}{\lambda_p^2 (\lambda_c + i\lambda)} \right)^{1/2} \quad (1)$$

Methodology

A monochromatic light source emits light with λ of 633 nm, and a computer-linked spectrometer detects the corresponding statistics. The SPs are generated at the metal-dielectric (M-D) interface due to the oscillations of quanta-free electrons. The attenuated total reflection (ATR) method is applied to the prism-based SPR in order to excite the surface plasmon waves (SPW) at the M-D interface [43]. As a

result, the SPW resists the plasmon’s light energy and converts it into reflected light. In the event of reflectance, the SPW excites the evanescent wave at the M-D interface. The incident light is reflected at the P-M interface after passing through the prism and forming the evanescent wave. This evanescent wave propagates along the x-axis through the AIAs layer with the propagation constant (PC) of an incident wave vector (k_x). The intensity of the evanescent wave deteriorates exponentially with the perpendicular direction to the P-M interface [44]. The less intensity of the reflectance light or minimum reflectance (R_{min}) occurs at the resonance condition, where the vectors of the EMW are equal to the SPWs. The R_{min} transpires where the PC of k_x and the wave vector of SPs (k_{spw}) are matched, and this condition is directed by the theta. This condition is entitled the resonance condition, and its mathematical expressions are mentioned in Eq. (2) and (3) [28, 45]. Therefore, the resonance dip or angle (the dip or angle where the R_{min} is accomplished) transmutes according to the minute RI fluctuations of the employed materials in the SPR sensor structure [46].

$$k_x = k_{SPW} \tag{2}$$

$$\frac{2\pi}{\lambda_{633}} (n_{prism} \sin \theta) = \frac{2\pi}{\lambda_{633}} \sqrt{\frac{n_{Ag}^2 n_s^2}{n_{Ag}^2 + n_s^2}} \tag{3}$$

n_{prism} , n_{Ag} and n_s are the RI of the prism, Ag and sensing medium, respectively. Equation (4) evaluates the SPR resonance angle (θ_{SPR}), which shows the angle where the R_{min} is obtained [29].

$$\theta_{SPR} = \text{asin} \sqrt{\frac{n_{Ag}^2 n_s^2}{n_{prism}^2 (n_{Ag}^2 + n_s^2)}} \tag{4}$$

The angular interrogation technique is considered for the study of the proposed SPR composition. Moreover, we have utilized the Fresnel model analysis of multilayer reflection theory and transfer matrix method (TMM) to investigate the reflectivity of the P–polarized incident light wave. The SPR curve shows the relation between the reflectivity intensity (R_p) of the sensor and the incidence angle. The mathematical expression for measuring the R_p and reflection coefficient (r_p) are represented in Eqs. (5) and (6), respectively [26, 47].

$$R_p = r_p r_p^* = |r_p|^2 \tag{5}$$

$$r_p = \frac{(H_{11} + H_{12}n_N) - (H_{21} + H_{22}n_N)}{(H_{11} + H_{12}n_N) + (H_{21} + H_{22}n_N)} \tag{6}$$

Equation (7) describes the description of the transverse RI (t_L) for the corresponding Lth layer [48].

$$t_L = \left[\begin{matrix} \mu_L \\ \epsilon_L \end{matrix} \right]^{1/2} \cos \theta_L = \sqrt{\frac{\epsilon_L - (n_{BK7} \sin \theta)^2}{\epsilon_L^2}} \tag{7}$$

In Eq. (6), H is the characteristics matrix of the sensor and mathematically represented in Eq. (8) [48].

$$H_{if} = \left[\prod_{k=2}^{N-1} \begin{pmatrix} \cos \beta_L & -i \sin \beta_L \\ -i n_L \sin \beta_L & \cos \beta_L \end{pmatrix} \right]_{if} = \begin{bmatrix} H_{11} & H_{12} \\ H_{21} & H_{22} \end{bmatrix} \tag{8}$$

Furthermore, the arbitrary stage constant (β_L) for Lth layer is represented in Eq. (9) [49].

$$\beta_L = \frac{2\pi}{\lambda} n_L \cos \theta_L (z_L - z_{L-1}) = \frac{2\pi}{\lambda} d_L \sqrt{\epsilon_L - (n_{BK7} \sin \theta)^2} \tag{9}$$

And, Eq. (10) exhibits the wave impedance (z_L) of Lth layer [38].

$$z_L = \frac{k_x n_L \cos \theta_L}{(2\pi c / \lambda_{633}) \epsilon_L^2} \tag{10}$$

Finally, the input angle (θ_L) for a Lth layer evaluates by using the Eq. (11) [50].

$$\theta_L = \text{acos} \sqrt{1 - (n_{L-1} / n_L) (\sin \theta)^2} \tag{11}$$

ϵ_L , μ_L and d_L permittivity, permeability and thickness of Lth layer.

SPR performance parameter

The S plays major role for a high performance SPR biosensor, and it is defined as the ratio of variation in the SPR resonance angle ($\nabla \theta_{SPR}$) to variation in the RI (∇n) [28]. The higher S performance of a sensor with minute variation in analyte (biomolecules) concentration is demonstrated that the sensor has better sensing capabilities since it can detect minute RI variations in the structure. In addition, we compute the performance of dip of figure of merit (DFOM), which describe the ratio of S to R_{min} . The performances of DFOM are demonstrated the noise impact in a sensor, quality and accuracy of the product. An optical fibre SPR desires all these parameters as high as possible. The mathematical modeling for computing the performance S and DFOM are represented in Eqs. (12) and (13) [11, 31].

$$\text{Sensitivity (S)} = \frac{\text{change in resonance angle } (\nabla \theta_{res})}{\text{change in refractive index } (\nabla n)} \quad (^\circ / \text{RIU}) \tag{12}$$

Dip of Figure of Merit (DFOM)

$$= \frac{S}{\text{Minimum reflection } (R_{\min})} \tag{13}$$

Results and discussion

The proposed work has been investigated into two significant ways. In first part, this investigation analyzes the optimal performance in terms of prism-based structure with AIAs. In the second part, the optimized prism structure is further analyzed using different combinations of dielectric materials in order to show the impact of AIAs on S. Therefore, different prism-based structures and their configurations are defined in Table 2 to achieve the optimized structure for urea detection.

Optimized performance of the K-prism-based structure and AIAs’s thickness

In this section, the performance shows the optimization of prism-based structure and the AIAs layer thickness. The iteration method of Fresnel’s reflectivity (R_p) mode is considered for this investigation [27]. Moreover, less R_{\min} and higher S are required to optimize the structure’s layer thickness [28, 30]. In addition, we also evaluated the DFOM performance for this investigation. The R_{\min} occurs at the resonance condition that shows the maximum light energy transfer to the SPW, which can directs toward enhancing the SPR field. To optimize the prism-based structure, three prism-based structures are considered with AIAs as mentioned in Table 2. Therefore, Fig. 2a to c presents the reflectance responses for structure-1, 2 and 3 in order to optimize the suitable prism structure and thickness of the AIAs. All of the responses in Fig. 2a to c are plotted for the Ag, BaTiO₃ and BP thicknesses of 50 nm, 5 nm and 0.53 nm, respectively, because of they provide a lower damping effect as well as a lower absorption loss [11]. Figure 2a represents the SPR reflectance responses for structure-1 at different AIAs thicknesses (1–6 nm with an interval of 1 nm).

In this analysis, the S and DFOM performances are computed using Eqs. (12) and (13) for small RI change (Δn) of 0.007 in the the urea sample. The achieved R_{\min} values are 0.0438, 0.0367, 0.0244, 0.0054, 0.0639 and 0.8848, and the

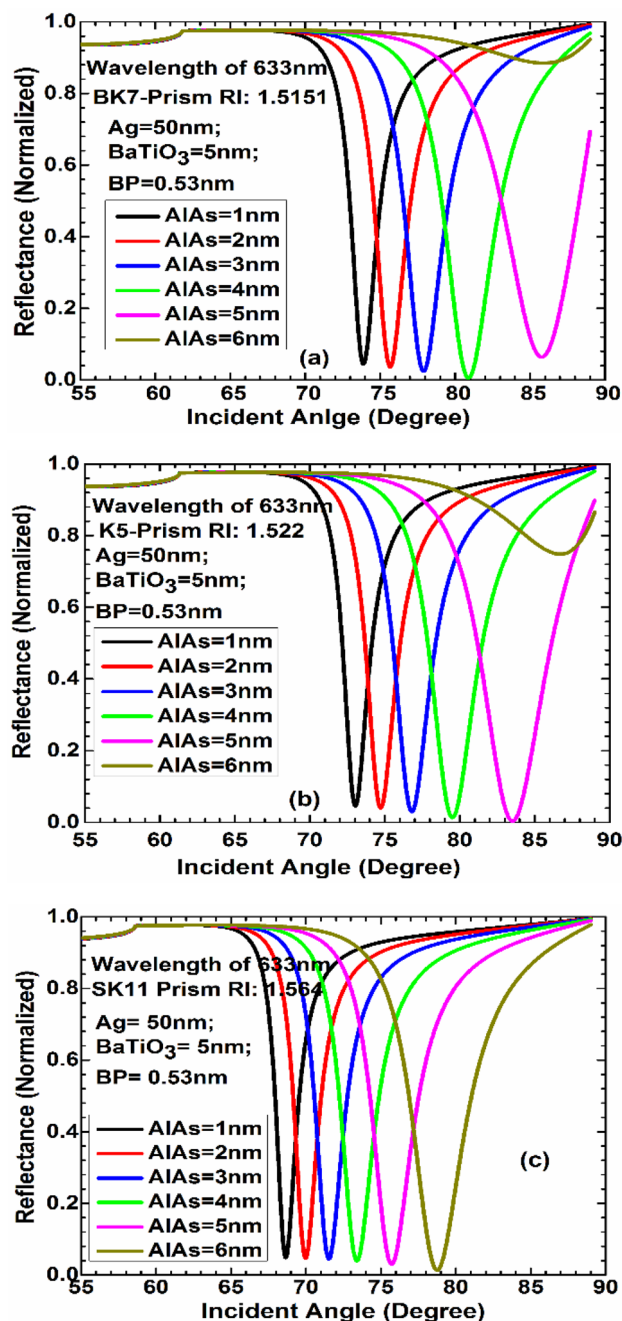


Fig. 2 Optimization of prism and thickness of AIAs by employing angular interrogation method. **a** Reflectance curves for different AIAs thickness using BK7 prism (RI: 1.5151) **b** Reflectance curves for different AIAs thickness using K5 prism (RI: 1.522) **c** Reflectance curves for different AIAs thickness using SK11 prism (RI: 1.564)

Table 2 Different types of SPR biosensors for optimizing the prism performance

Structure no	Structure name (RI)	Configuration
1	BK7-based SPR (1.515)	BK7 Prism(1)/ Ag(2)/ AIAs(3)/ BaTiO ₃ (4)/ BP(5)/ Sensing layer(6)
2	K5-based SPR (1.522)	K51 Prism(1)/ Ag(2)/ AIAs(3)/ BaTiO ₃ (4)/ BP(5)/ Sensing layer(6)
3	SK11-based SPR (1.564)	SK11 Prism(1)/ Ag(2)/ AIAs(3)/ BaTiO ₃ (4)/ BP(5)/ Sensing layer(6)

sensitivities are 170, 194.29, 234.29, 325.71, 194.29 and 171.49°/RIU for the assigned AIAs thicknesses, respectively. Similarly, the achieved DFOMs are 3881.28, 5290.00, 9602.05, 60,316.67, 3040.53 and 193.82 for the assigned AIAs thicknesses, respectively. The less R_{min} is achieved as a consequence of the spatial extension of SPs in a medium [43]; and high R_{min} is transpired due to the attenuation or damping of electromagnetic wave's affect and RI of dielectric material i.e., AIAs [34]. The asymmetry in the achieved S and DFOM because of the biomolecules binding on the sensing surface to detect the change in the sensing medium's RI [43, 49]. Moreover, the higher S is accomplished due to the less damping that offers the high evanescent field's penetration depth (PD) of the SPW and the top layer's high absorption capability [43].

Similarly, Fig. 2b exhibits the SPR reflectance responses for structure-2 (proposed K5 prism-based SPR) at different AIAs thicknesses (1–6 nm with the interval of 1 nm). The obtained R_{min} values are 0.0457, 0.0401, 0.0300, 0.0035 and 0.7480, and the sensitivities are 160, 180, 212.86, 277.14, 452.86 and 151.43°/RIU for the given AIAs thicknesses, respectively. Similarly, the accomplished DFOMs are 3501.09, 4488.78, 7095.33, 20,995.45, 129,388.57 and 202.45 for respected AIAs thicknesses. At the AIAs thickness of 5 nm, the sensor shows high sensing capability that accomplishes the huge S and DFOM performances. Beyond the 5 nm thickness of AIAs, the S and DFOM performances are decaying because of the low PD and damping effect. Finally, Fig. 2c explores the SPR reflectance responses for structure-3 at different AIAs thicknesses (1–6 nm with the interval of 1 nm). The attained R_{min} values are 0.0487, 0.0472, 0.0446, 0.03035 and 0.0136, and the sensitivities are 125.71, 137.14, 151.43, 165.71, 198.57 and 257.14°/RIU for the individual AIAs thicknesses. Similarly, the obtained DFOMs are 2581.31, 2905.51, 3395.29, 4184.60, 65,553.47 and 18,907.35 for respected AIAs thicknesses.

In summary, the computed parameters of R_{min} , S and DFOM for Fig. 2 are reported in Table 3, whereas Fig. 3a, b and c are shown their graphical representations. Since the adequate SPR sensor should have less R_{min} and high S, Fig. 3 and Table 3 have witnessed that structure-2 grants the required SPR parameters (low R_{min} and high S and DFOM

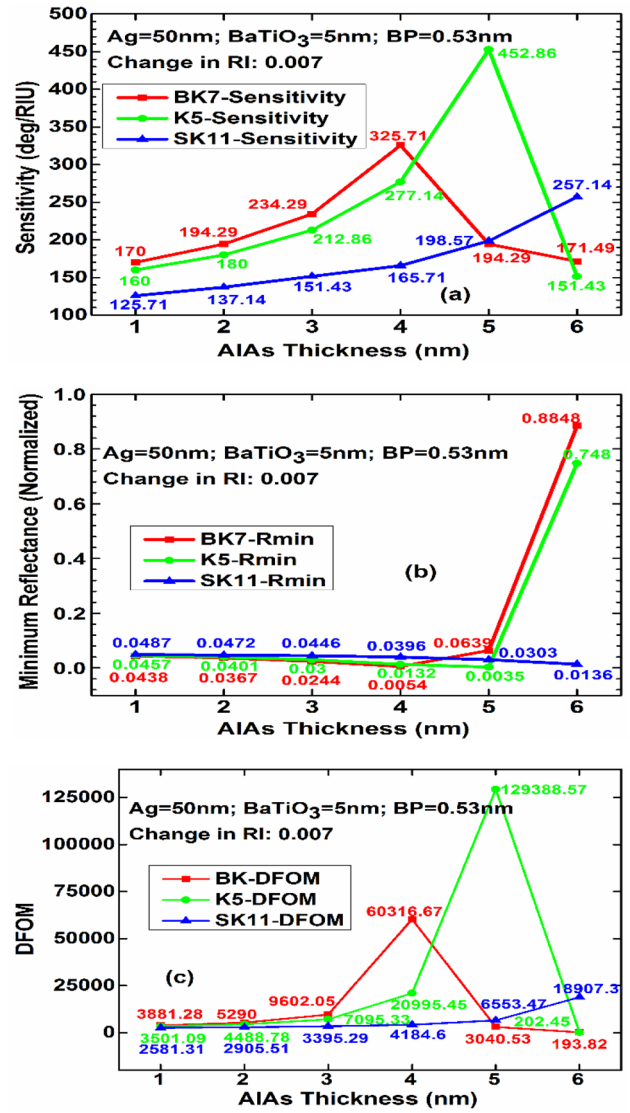


Fig. 3 Graphical representation of computed performance in terms of S a, R_{min} b and DFOM c with respect to the AIAs thickness for different types of prisms

performances) compared to structure-1 and 3. Due to the increment in the biomolecules binding on the sensing surface at 5 nm thickness of AIAs, the sensor accomplished higher S. Therefore, we conclude that the adequate SPR

Table 3 Measuring performance of R_{min} , sensitivity and DFOM for different prisms and AIAs thicknesses

AIAs thickness	BK7 Prism			K5 Prism			SK11 Prism		
	R_{min}	S	DFOM	R_{min}	S	DFOM	R_{min}	S	DFOM
1 nm	0.0438	170	3881.28	0.0457	160	3501.09	0.0487	125.71	2581.31
2 nm	0.0367	194.29	5290.00	0.0401	180	4488.78	0.0472	137.14	2905.51
3 nm	0.0244	234.29	9602.05	0.0300	212.86	7095.33	0.0446	151.43	3395.29
4 nm	0.0054	325.71	60,316.67	0.0132	277.14	20,995.45	0.0396	165.71	4184.60
5 nm	0.0639	194.29	3040.53	0.0035	452.86	129,388.57	0.0303	198.57	6553.47
6 nm	0.8848	171.49	193.82	0.7480	151.43	202.45	0.0136	257.14	18,907.35

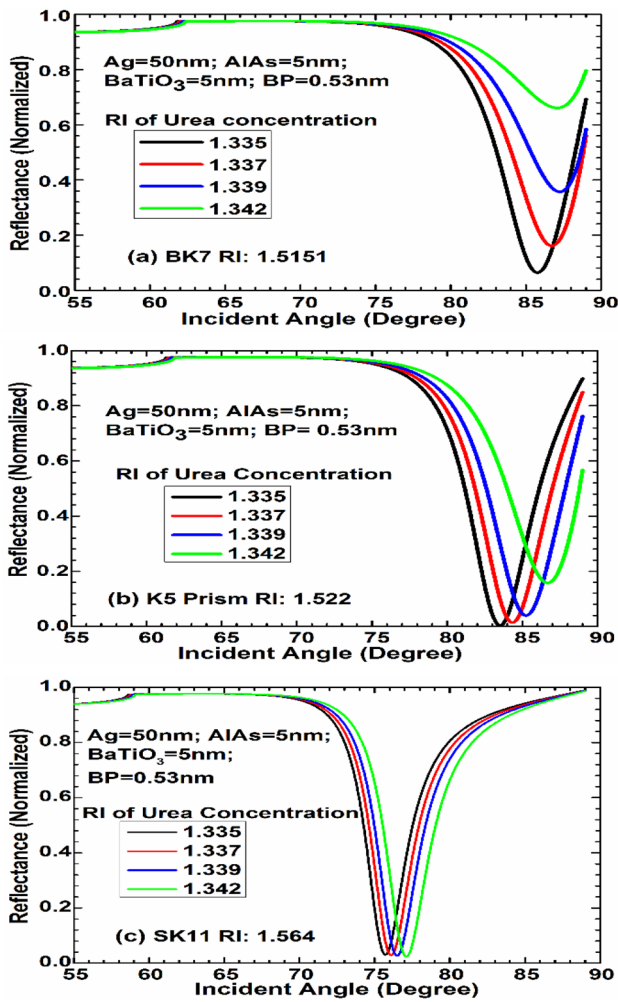


Fig. 4 a Reflectance curves for different concentration of urea using BK7 prism (RI: 1.5151) b Reflectance curves for different concentration of urea using K5 prism (RI: 1.522) c Reflectance curves for different concentration of urea using SK11 prism (RI: 1.564)

performance furnishes at the AlAs thickness of 5 nm by employing the K5 prism in the proposed SPR structure.

Optimized performance of the K-prism with respect to urea concentration

The performance here shows the optimization of the K5 prism structure in another significant way, i.e., with respect

to the urea concentration. Therefore, Fig. 4a–c presents the reflectance responses in terms of an angle for three prism-based structures at different refractive indexes of the urea samples. For performance comparison, all responses are plotted at constant thicknesses of Ag, AlAs, BaTiO₃ and BP are 50 nm, 5 nm, 5 nm and 0.53 nm, respectively. The sensing medium determines the refractive indexes with urea presence, having the RI of 1.337, 1.339 and 1.342, at the urea concentrations of 0.625 gm/dl, 2.5 gm/dl and 5 gm/dl, respectively. The RI for normal urea is decisive as 1.335 [3, 43]. Figure 4a–c have the identical sensing refractive indexes of the urea samples. Figure 4a represents the SPR responses in terms of reflectance for structure-1 at different urea refractive indices. The R_{min} (resonance angle) comprises of 0.0639 (85.77°), 0.1613 (86.77°), 0.3571 (87.23°) and 0.6613 (87.03°) for respective RIs of urea samples. The sensitivities are measured for three different RI changes (Δn) amounts of the sensing medium, such as 0.002, 0.004 and 0.007. Therefore, the achieved sensitivities of 500, 365 and 180°/RIU for the BK7 prism at the respective Δn amounts of the sensing medium. Similarly, Fig. 4b shows the SPR reflectance responses for structure-2. The acquired R_{min} of 0.0035 (83.52°), 0.0139 (84.34°), 0.0394 (85.26°) and 0.1576(86.69°) for registered urea RIs, and sensitivities of 410°/RIU, 435°/RIU and 452.85°/RIU for the respected Δn values of the sensing region. Finally, Fig. 4c presents the reflectance responses for structure-3 at different urea refractive indexes. The obtained R_{min} (resonance angle) values are 0.0303 (75.73°), 0.0284 (76.10°), 0.02647 (76.51°) and 0.0232 (77.12°) for allotted urea RIs, and the sensitivities are 180°/RIU, 195°/RIU and 198.57°/RIU for the respective Δn values of sensing medium, respectively. The performances of R_{min} , sensitivities and DFOM for Fig. 4a–c are reported in Table 4, whereas Fig. 5a–b exhibits their graphical representations.

In summary, the S of structure-1 is decaying with corresponds to the urea sample’s RI, and it is inversely proportional to the Δn of urea presence of the sensing medium due to low dispersion (i.e., low RI variation) [44]. The S performance of Fig. 4b shows that structure-2’s S is increasing significantly and directly proportional to the very small Δn amounts of urea sample, which is the researchers’ ultimate goal [30]. Structure-3 furnishes lower S performance due to low absorption capability and lower light coupling at

Table 4 Measuring performance of R_{min} , DFOM and sensitivities for different prisms and urea RIs

Urea RI	BK7 Prism			K5 Prism			SK11 Prism		
	R_{min}	S (°/RIU)	DFOM	R_{min}	S (°/RIU)	DFOM	R_{min}	S (°/RIU)	DFOM
1.335	0.0639	–	–	0.0035	–	–	0.0303	–	–
1.337	0.1613	500	7824.73	0.0139	410	117,142.86	0.0284	185	6105.51
1.339	0.3571	365	5712.05	0.0394	435	124,285.71	0.02647	195	6435.64
1.342	0.6613	180	2816.90	0.1576	452.85	129,388.57	0.0232	198.57	6553.47

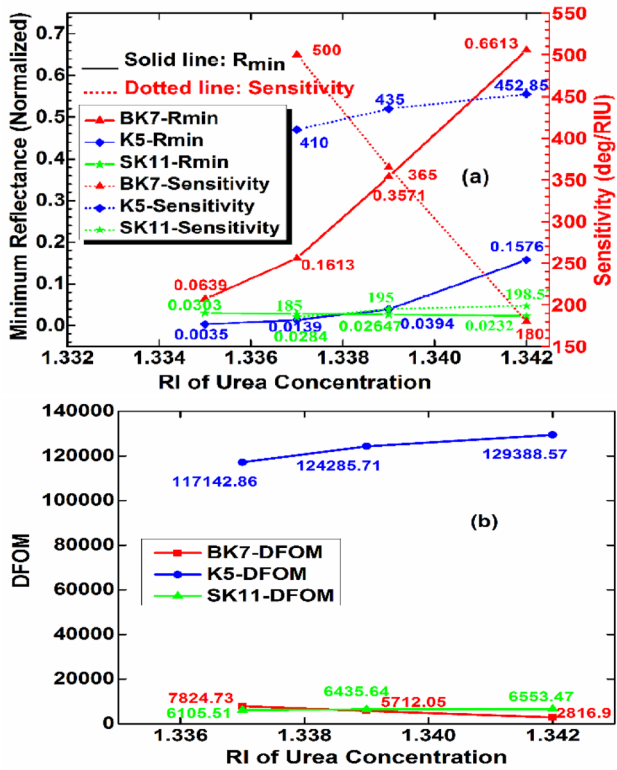


Fig. 5 Performance of R_{min} and S **a**, and DFOM **b** for different types of prisms at different RIs of urea concentration

the P-M interface. From these observation, it can be easily stated that the massive performances, such as less R_{min} and higher increment of S performances, are transpired at AIAs thickness of 5 nm for the K5 prism-based SPR (structure-2) compared to other two prism-based SPR sensors, i.e., structure-1 and 3.

Impact of AIAs dielectric material in the proposed SPR sensor

Earlier, we discussed the optimization of the suitable prism-based structure and AIAs thickness for the proposed SPR sensor, demonstrating the K5-based SPR offers better performance at AIAs thickness of 5 nm. In order to show the impact of AIAs in the proposed structure, the optimized prism structure analyzed the S performance using three different combinations of dielectric materials: AIAs-based sensor, BP-based and BaTiO₃-based sensor. The structure name and its configurations have been presented in Table 5.

Table 5 Different structure names and configurations of the proposed SPR biosensor

Structure name	Configuration
1. BP-based SPR	K5 Prism(1)/ Ag(2)/BP(5)/Sensing layer(6)
2. BaTiO ₃ -based SPR	K5 Prism(1)/ Ag(2)/BaTiO ₃ (4)/ BP(5)/ Sensing layer(6)
3. AIAs-based SPR	K5 Prism(1)/ Ag(2)/AIAs(3)/ BaTiO ₃ (4)/ BP(5)/ Sensing layer(6)

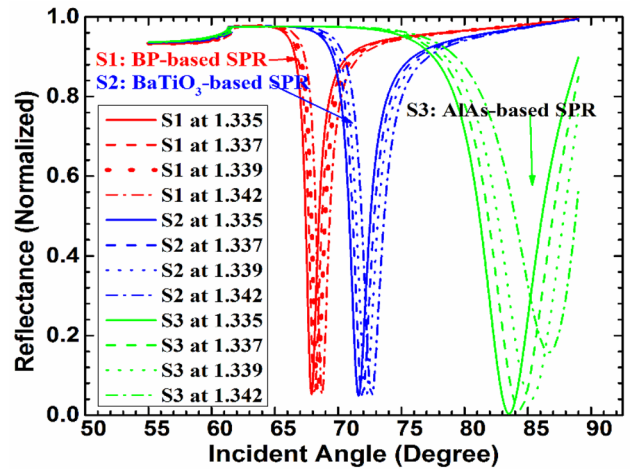


Fig. 6 Reflectance responses for three different structures of the proposed SPR sensor, such as BP-based, BaTiO₃-based and AIAs-based

The reflectance intensity performances in terms of an angle for just the above-defined configurations (as mentioned in Table 5) are presented in Fig. 6. Where the red, blue and green colors signify the BP-based, BaTiO₃-based and AIAs-based sensors, respectively. Moreover, the solid, dash, dotted and dash-dot lines are represented for the sensing RI of 1.335, 1.337, 1.339 and 1.342, respectively. This study has considered the RI of 1.335 as a reference for the S measurement.

The measured parameters as R_{min} , θ_{res} and S of Fig. 6 are presented in Table 6 for observing the optimal performance. The obtained resonance angles are directly proportional to the structure to structure as well as sensing RI. The AIAs-based sensor has accomplished low R_{min} values compared to the BP-based and BaTiO₃-based sensors due to less damping effect. It signifies the maximum energy of an incident light transfers to the SPW that can enhance the sensor’s performance. In summary, the performance is explored that the BaTiO₃-based sensor has a better S than the BP-based sensor due to enhanced properties of BaTiO₃ as found in the literature. Also, this enhancement occurs as a consequence of its high molar mass of the substance (233.192 g/mol), crystal forms of a perovskite structure and high-density value (6.02 g cm⁻³) [22, 44]. Moreover, the AIAs-based sensor is accomplished a noteworthy S compared with the BaTiO₃-based sensor due to the high penetration depth of SPW, high dielectric RIs of AIAs. Furthermore, by depositing the promising 2D family materials of BaTiO₃, BP on the AIAs

Table 6 Comparison of SPR parameters including R_{\min} , resonance angle and sensitivity of AIAs-based sensor with other two structures i.e., BP and BaTiO₃-based sensor

Structure name	Sensing RI	BP-based SPR	BaTiO ₃ -based SPR	AIAs-based SPR
Minimum Reflectance (R_{\min})	1.335	0.0525	0.0492	0.0035
	1.337	0.0525	0.0484	0.0139
	1.339	0.0525	0.0468	0.0394
	1.342	0.0529	0.0481	0.1576
Resonance angle (θ_{res}) (°)	1.335	67.9	71.61	83.52
	1.337	68.14	71.91	84.34
	1.339	68.38	72.22	85.26
	1.342	68.72	72.66	86.69
Sensitivity (S)°/RIU	($\nabla n = 0.002$)	120	150	410
	($\nabla n = 0.004$)	120	152.5	435
	($\nabla n = 0.007$)	117.14	150	452.86
Dip of FOM (DFOM)	($\nabla n = 0.002$)	2285.71	3048.78	117,142.86
	($\nabla n = 0.004$)	2285.71	3099.59	124,285.71
	($\nabla n = 0.007$)	2231.24	3048.78	129,388.57

surface, the absorption molecule capability is strengthened, which can prevent adsorption, environmental effects and achieve low absorption loss [12].

Also, Fig. 7a–c depict the graphical representation of measured SPR performances in terms of R_{\min} , S and DFOM of different configurations of the proposed SPR sensor. Finally, these performances are demonstrated that the AIAs-based sensor is furnished the massive S than the BP and BaTiO₃-based sensors, respectively, i.e., 3.42 and 2.73 times higher at ∇n of 0.002; 3.63 and 2.85 times higher at ∇n of 0.004; 3.87 and 3.02 times higher at ∇n of 0.007. Therefore, the proposed SPR sensor supplies superior S for urea detection, and it contributes a new platform for bio-sensing applications.

In addition, the study investigates the performance of the electric field intensity enhancement factor (EFIEF) for all structures. The EFIEF is a parameter that shows the origin of the S improvement and can be expressed as Eq. (14) [50].

$$EFIEF = \frac{\varepsilon_1}{\varepsilon_n} |t|^2 \quad (14)$$

The field intensity is inversely proportional to reflectivity that means the field intensity's extreme value is the reflectivity's minimal value. Due to the less R_{\min} , the maximum SPs excitation transpires at the place of strong EFIEF. The performance of EFIEF with respect to an incident angle for all structures at sensing RI of 1.335 is evaluated using the Eq. (14) [50] and shown in Fig. 8. The maximum achieved EFIEF values are 1.5166, 1.5272 and 1.6775, and corresponding to the sensitivities are 120, 152.5 and 452.86 deg/RIU for BP-based, BaTiO₃-based and AIAs-based sensors, respectively. Therefore, it is clear observed that the AIAs-based sensor provides higher EFI than the other structures,

and also the greater EFIEF performance shows a better S factor.

Comparative study of proposed work performance and existing work

Finally, this section shows the comparative study of proposed work performance with existing works, as shown in Table 7. FWHM-based parameters, such as quality factor (QF) and detection accuracy (DA), are also measured using Eqs. (15) and (16) [28]. It is noticed that the proposed work is accomplished higher S of 452.86°/RIU and QF of 93.37 compared to existing works, where the literature highlighted a higher S acts a key role in the SPR research field. Moreover, the proposed work is computed the performance of DA of 0.65 and DFOM of 29,496.40, which show good accuracy and quality of the product. Therefore, the proposed SPR sensor can be used to facilitate a higher performance in the urea detection process.

$$\text{Quality Factor (QF)} = \frac{S}{\text{FWHM}} (\text{RIU}^{-1}) \quad (15)$$

$$\text{Detection Accuracy (DA)} = \frac{\nabla \theta_{\text{res}}}{\text{FWHM}} \quad (16)$$

Conclusion

High performing SPR sensor is proposed employing the K5 prism structure with AIAs for urea detection in this paper. The proposed SPR sensor structure comprises of Ag,

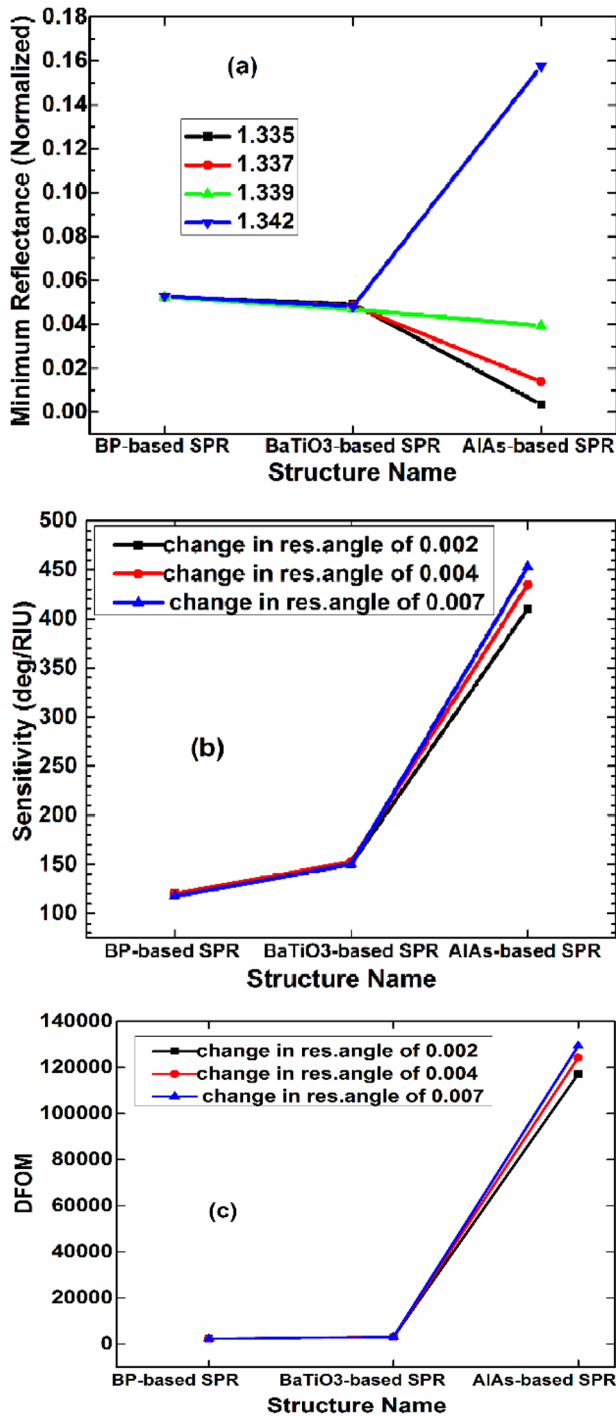


Fig. 7 Graphical representation of measured performance parameters for different structures of the proposed SPR sensor **a** R_{min} **b** S and **c** DFOM

BaTiO₃ and BP in order to achieve a high SPR ratio, low dielectric losses and high adsorption capability. Initially, the performance optimization has been carried out for the K5

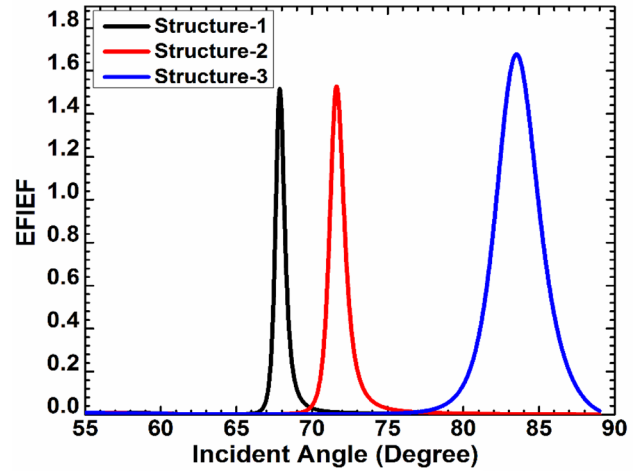


Fig. 8 The performance of EFIEF with respect to the angle for all structures at the normal urea sample RI of 1.335

prism-based structure and AIAs thickness. For the optimization process, the reflectance responses are plotted, which show a low R_{min} with higher resonance shift that leads to a higher sensitivity. In the first investigation, the prism-based structure is optimized, and it is found that maximum sensitivity of structure-2 (i.e., proposed structure) is 452.86 °/RIU, which is 2.28 and 2.33 times higher than structure-1 and 3 at the optimized AIAs thickness of 5 nm, respectively. In addition, the structure is achieved a higher DFOM performance of 129,388.57, which shows better quality and accuracy product. The enhanced performance of the proposed structure is validated with respect to the urea RI as a second investigation of the study. In the third investigation, an impact of AIAs in the proposed sensor has been shown. Results show that the sensitivity of the proposed SPR sensor is increased by 3.42 and 2.73 times higher than the BP and BaTiO₃-based sensors, respectively. Finally, the comparative study is witnessed that the proposed work facilitates a higher sensitivity of 452.86 °/RIU and QF of 93.37 RIU⁻¹ and heightened the DA of 0.65 and DFOM of 129,388.57 performances compared to existing works. Therefore, the proposed K5 prism-based SPR sensor with AIAs can be used for urea detection with high performance and treated as an excellent candidate for biomedical sensing applications.

Table 7 SPR performance comparison of proposed work and existed work for urea detection

References	SPR Structure	Sensitivity (°/RIU)	QF (RIU ⁻¹)	DA	DFOM
[42]	BSG prism-Cu-Graphene-Sensing	32.653	–	–	–
[6]	BK7 prism-Chr-Au-Graphene-MoS ₂ -Sensing	85.08	–	–	–
[7]	Soda lima prism-Chr-Al ₂ O ₃ -MoS ₂ -Graphene-Sensing	202.02	–	–	–
[3]	Soda lima prism-Chr-Au-MoS ₂ -Graphene-Sensing	230	–	–	–
[51]	BSG prism-Au-GeO ₂ -GaP-Sensing	280	41.36	–	–
Proposed work	K5 prism-Ag-AlAs- BaTiO ₃ -BP-Sensing	452.86	93.37	0.65	29,496.40

Acknowledgements This research did not receive any specific grant from funding agencies in the public, commercial or not-for-profit sectors.

References

- M. Eghbali, A. Farahbakhsh, A. Rohani, A.N. Pour, Urea biosensor based on immobilization of urease on ZnO nanoparticles. *Orient. J. Chem.* **31**, 1237–1242 (2015). <https://doi.org/10.13005/ojc/310284>
- J.F. Masson, Surface plasmon resonance clinical biosensors for medical diagnostics. *ACS Sens.* **2**, 16–30 (2017). <https://doi.org/10.1021/acssensors.6b00763>
- N.A. Jamil, P.S. Menon, F.A. Said, K.A. Tarumaraja, G.S. Mei, B.Y. Majlis, Graphene-based surface plasmon resonance urea biosensor using Kretschmann configuration. *IEEE (RSM)* (2017). <https://doi.org/10.1109/RSM.2017.8069122>
- S. Pal, A. Verma, J.P. Saini, Y.K. Prajapati, Sensitivity enhancement using silicon-black phosphorus-TDMC coated surface plasmon resonance biosensor. *Inst. Eng. Techn. Optoelec.* **13**, 196–201 (2019). <https://doi.org/10.1049/iet-opt.2018.5023>
- B.D. Gupta, R.K. Verma, Surface plasmon resonance-based fiber optic sensors: principle, probe designs, and some applications. *J. Sens.* (2009). <https://doi.org/10.1155/2009/979761>
- N.A. Jamil, N.B. Khairulazdan, P.S. Menon, A.R. Zain, A.A. Hamzah, B.Y. Majlis, Graphene-MoS₂ SPR-based biosensor for urea detection. *IEEE (ISESD)* (2018). <https://doi.org/10.1109/ISESD.2018.8605491>
- N. A. Jamil, P. S. Menon, G. S. Mei, S. Shaari, B. Y. Majlis, “Urea biosensor utilizing graphene- MoS₂ and Kretschmann-based SPR”, *IEEE InTENCON*, 1973–1977 (2017). <https://doi.org/10.1109/TENCON.2017.8228183>
- J. Homola, Surface plasmon resonance based sensors. *Chem. Sens. Biosen.* **4**, 45–67 (2006). <https://doi.org/10.1007/5346-014>
- H. Fu, S. Zhang, H. Chen, J. Weng, Graphene enhances the sensitivity of fiber optic surface plasmon resonance biosensor. *IEEE Sens.* **15**, 5478–5482 (2015). <https://doi.org/10.1109/JSEN.2015.2442276>
- K.L. Lee, C.W. Lee, W.S. Wang, P.K. Wei, Sensitive biosensor array using surface plasmon resonance on metallic nanoslits. *J. Biomed. Opt.* **12**, 044023 (2007). <https://doi.org/10.1117/1.277296>
- L. E. Ronald, “Multiwavelength Surface Plasmon Resonance Sensor Designs for Chemical and Biochemical Detection”, PHD thesis, Dept. of Chemistry, Virginia Polytechnic Institute and State University, Ontario, Canada, (2013).
- S.H. Choi, Y.L. Kim, K.M. Byun, Graphene-on-silver substrates for sensitive surface plasmon resonance imaging biosensors. *Opt. Exp.* **19**, 458–466 (2011). <https://doi.org/10.1364/OE.19.000458>
- R. Kumar, S. Pal, Y. K. Prajapati, S. Kumar, J. P. Saini, “Sensitivity Improvement of a MXeneimmobilized SPR Sensor with G-doped-ZnO for Biomolecules Detection”, *IEEE Sensors*, (2022).
- A. Verma, A.K. Sharma, Y.K. Prajapati, On the sensing performance enhancement in SPR-based Biosensor using specific two-dimensional materials (Borophene and Antimone). *Opt. Mater.* **119**, 111355 (2021). <https://doi.org/10.1016/j.optmat.2021.111355>
- V.K. Verma, S. Pal, C. Rizal, Y.K. Prajapati, Tunable and sensitive detection of cortisol using anisotropic phosphorene with a surface plasmon resonance technique: numerical investigation. *Magnetochem.* **8**(3), 31 (2022). <https://doi.org/10.3390/magnetochem8y8030031>
- A. Verma, A. Prakash, R. Tripathi, Sensitivity enhancement of surface plasmon resonance biosensor using graphene and air gap. *Opt. Comm.* **357**, 106–112 (2015). <https://doi.org/10.1016/j.optcom.2015.08.076>
- A.K. Sharma, A.K. Pandey, Blue phosphorene/ heterostructure based SPR sensor with enhanced sensitivity. *IEEE Phot. Techn. Lett.* **30**, 595–598 (2018). <https://doi.org/10.1109/LPT.2018.2803747>
- R. Kumar, A.S. Kushwaha, M. Srivastava, H. Mishra, S.K. Srivastava, Enhancement in sensitivity of graphene-based zinc oxide assisted bimetallic surface plasmon resonance (SPR) biosensor. *Appl. Phys. A Mater. Sci. Proc.* **124**, 235 (2018). <https://doi.org/10.1007/s00339-018-1606-5>
- S. Fouad, N. Sabr, Z.A.Z. Jamal, P. Poopalan, Surface plasmon resonance sensor sensitivity enhancement using gold-dielectric material. *Int. J. Nanoelectron. Mater.* **10**, 149–158 (2017)
- L. Liu, M. Wang, L. Jiao, T. Wu, F. Xia, M. Liu, W. Kong, L. Dong, M. Yun, Sensitivity enhancement of a graphene–barium titanatebased surface plasmon resonance biosensor with an Ag–Au bimetallic structure in the visible region. *J. Opt. Soc. Am. B* **36**, 1108–1116 (2019). <https://doi.org/10.1364/JOSAB.36.001108>
- P. Sun, M. Wang, L. Liu, L. Jiao, W. Du, F. Xia, M. Liu, W. Kong, L. Dong, M. Yun, Sensitivity enhancement of surface plasmon resonance biosensor based on graphene and barium titanate layers. *Appl. Surf. Sci.* **475**, 342–347 (2019). <https://doi.org/10.1016/j.apsusc.2018.12.283>
- M.S. Rahman, M.R. Hasan, K.A. Rikta, M.S. Anower, A novel graphene coated surface plasmon resonance biosensor with tungsten disulfide (WS₂) for sensing DNA hybridization. *Opt. Mater.* **75**, 567–573 (2018). <https://doi.org/10.1016/j.optmat.2017.11.013>
- S.Y. Cho, Y. Lee, H.J. Koh, H. Jung, J.S. Kim, H.W. Yoo, J. Kim, H.J. Jung, Superior chemical sensing performance of black phosphorus: comparison with and graphene. *Adv. Mater.* **28**, 7020–7028 (2016). <https://doi.org/10.1002/adma.201601167>
- N. Mao, J. Tang, L. Xie, J. Wu, B. Han, J. Lin, S. Deng, W. Ji, H. Xu, K. Liu, L. Tong, Optical anisotropy of black phosphorus in the visible regime. *Am. Chem. Soc.* **138**, 300–305 (2016). <https://doi.org/10.1021/jacs.5b10685>

25. L. Wu, J. Guo, Q. Wang, S. Lu, X. Dai, Y. Xiang, D. Fan, Sensitivity enhancement by using few-layer black phosphorus-graphene/TMDCs heterostructure in surface plasmon resonance biochemical sensor. *Sen. Actua. B Chem.* **249**, 542–548 (2017). <https://doi.org/10.1016/j.snb.2017.04.110>
26. Y. Vasimalla, H.S. Pradhan, R.J. Pandya, SPR performance enhancement for DNA hybridization employing black phosphorus, silver, and silicon. *Appl. Opt.* **59**, 7299–7307 (2020). <https://doi.org/10.1364/AO.397452>
27. H. Bach, N. Neuroth, *The properties of optical glass* (Springer, Berlin, 1998). <https://doi.org/10.1007/978-3-642-57769-7>
28. P.B. Johnson, R.W. Christy, Optical constants of the noble metals. *Phys. Rev. B* **6**, 4370–4379 (1972). <https://doi.org/10.1103/PhysRevB.6.4370>
29. P.K. Maharana, T. Srivastava, R. Jha, On the performance of highly sensitive and accurate graphene-on-aluminum and silicon-based SPR biosensor for visible and near infrared. *Plasmonics* **9**, 1113–1120 (2014). <https://doi.org/10.1007/s11468-014-9721-4>
30. J.B. Maurya, Y.K. Prajapati, V. Singh, J.P. Saini, R. Tripathi, Performance of graphene-based surface plasmon resonance sensor using silicon layer. *Opt. Quant. Elect.* **47**, 3599–3611 (2015). <https://doi.org/10.1007/s11082-015-0233-z>
31. N. Mudgal, A. Saharia, A. Agarwal, G. Singh, ZnO and Bi-metallic (Ag–Au) layers based surface plasmon resonance (SPR) biosensor with BaTiO₃ and graphene for biosensing applications. *IETE J. Res.* (2020). <https://doi.org/10.1080/03772063.2020.1844074>
32. A. Pal, A. Jha, A theoretical analysis on sensitivity improvement of an SPR refractive index sensor with graphene and barium titanate nanosheets. *Optik* **231**, 166378 (2021). <https://doi.org/10.1016/j.ijleo.2021.166378>
33. B. Karki, A. Pal, Y. Singh, S. Sharma, Sensitivity enhancement of surface plasmon resonance sensor using 2D material barium titanate and black phosphorus over the bimetallic layer of Au, Ag, and Cu. *Opt. Comm.* **508**, 127616 (2022). <https://doi.org/10.1016/j.optcom.2021.127616>
34. A. Srivastava, R. Das, Y.K. Prajapati, Effect of perovskite material on performance of surface plasmon resonance biosensor. *IET Optoelectr.* **14**(5), 256–265 (2020). <https://doi.org/10.1049/iet-opt.2019.0122>
35. S.H. Wemple, J.M. Didomenico, I. Camlibel, Dielectric and optical properties of melt-grown. *J. Phys. Chem. Solids* **29**, 1797–1803 (1968). [https://doi.org/10.1016/0022-3697\(68\)90164-9](https://doi.org/10.1016/0022-3697(68)90164-9)
36. N. Mudgal, P. Yupapin, J. Ali, G. Singh, Graphene-Affinity Layer-Based Surface Plasmon Resonance (SPR) Biosensor for Pseudomonas Bacterial Detection. *Plasmonics* **2**, 1–9 (2020). <https://doi.org/10.1007/s11468-020-01146-2>
37. S. I. Ahmad, “Studies on some biophysical aspects of human renal excretory fluid”, Ph.D dissertation, Dept. Phys, JNTU, Hyderabad, India, 2010.
38. K.N. Shushama, M.M. Rana, R. Inum, M.B. Hossain, Sensitivity enhancement of graphene coated surface plasmon resonance biosensor. *Opt. Quantun. Electron.* **49**, 381 (2017). <https://doi.org/10.1007/s11082-017-1216-z>
39. M.S. Rahman, M.S. Anower, M.R. Hasan, M.B. Hossain, M.I. Haque, Design and numerical analysis of highly sensitive Au-MoS₂-graphene based hybrid surface plasmon resonance biosensor. *Opt. Comm.* **396**, 36–43 (2017). <https://doi.org/10.1016/j.optcom.2017.03.035>
40. S. Pal, A. Verma, Y.K. Prajapati, J.P. Saini, Figure of Merit Enhancement of Surface Plasmon Resonance Biosensor Using Ga-Doped Zinc Oxide in Near Infrared Range. *Phot. Sens.* (2020). <https://doi.org/10.1007/s13320-020-0583-4>
41. R. Çelen, Y. Ulcay, Baryum Titanatin Tekstilide Elektromanyetik Kalkanlama Uygulamalarında KullanIMI. *J. Ulu. Uni. Fac. Eng.* **23**, 29–44 (2018). <https://doi.org/10.17482/uumfd.398903>
42. F. A. Said, P. S. Menon, M. N. Nawi, A. R. Zain, A. Jalar, B. Y. Majlis, “Copper-graphene SPR-based biosensor for urea detection”, (ICSE) IEEE, 264–267 (2016). <https://doi.org/10.1109/SMELEC.2016.7573642>.
43. S. Pal, A. Verma, Y.K. Prajapati, J.P. Saini, Influence of black phosphorus on performance of surface plasmon resonance biosensor. *Opt. Quantun. Electron.* **49**, 403 (2017). <https://doi.org/10.1007/s11082-017-1237-7>
44. F.A. Said, P.S. Menon, T. Kalaivani, M.A. Mohamed, A. Abedini, S. Shaari, B.Y. Majlis, V. Retnasamy, FDTD analysis of structured metallic nanohole films for LSPR-based biosensor. *IEEE (RSM)* (2015). <https://doi.org/10.1109/RSM.2015.7355024>
45. H. Raether, “Surface plasmons on smooth surfaces, in Surface plasmons on smooth and rough surfaces and on gratings”, Springer, Berlin, pp 4–39 (1988)
46. W.M. Mukhtar, S. Shaari, A.A. Ehsan, P.S. Menon, Electrooptics interaction imaging in active plasmonic devices. *Opt. Mater. Exp.* **4**, 424 (2014). <https://doi.org/10.1016/j.snb.2012.07.015>
47. L. Wu, Y. Jia, L. Jiang, J. Guo, X. Dai, Y. Xiang, D. Fan D, Sensitivity improved SPR biosensor based on the MoS₂/graphene–aluminum hybrid structure. *J. Ligh. Techn.* **35**, 82–87 (2016). <https://doi.org/10.1109/JLT.2016.2624982>
48. B.J. Chu, D.R. Chen, G.R. Li, Q.R. Yin, Electrical properties of Na1/2Bi1/2TiO₃–BaTiO₃ ceramics. *J. Eur. Cer. Soc.* **22**, 2115–2121 (2002). [https://doi.org/10.1016/S0955-2219\(02\)00027-4](https://doi.org/10.1016/S0955-2219(02)00027-4)
49. I. Pockrand, Surface plasma oscillations at silver surfaces with thin transparent and absorbing coatings. *Surf. Sci.* **72**, 577–588 (1978). [https://doi.org/10.1016/0039-6028\(78\)90371-0](https://doi.org/10.1016/0039-6028(78)90371-0)
50. A. Shalabney, I. Abdulhalim, Electromagnetic fields distribution in multilayer thin film structures and the origin of sensitivity enhancement in surface plasmon resonance sensors. *Sens. Act. A* **159**, 24–32 (2010). <https://doi.org/10.3390/s20092445>
51. Y. Vasimalla, H. S. Pradhan, “Performance Enhancement of SPR sensor in NIR-Region for urea detection using MoS₂-Dielectric materials- MoS₂ based structure, in IEEE-ASIANCON, 1-4 (2021). <https://doi.org/10.1109/ASIANCON51346.2021.9544743>

Publisher’s Note Springer Nature remains neutral with regard to jurisdictional claims in published maps and institutional affiliations.